Chemical Physics Letters 693 (2018) 132–145

Contents lists available at ScienceDirect

Chemical Physics Letters

journal homepage: www.elsevier.com/locate/cplett

Research paper

Experimental and theoretical studies on tautomeric structures of a newly synthesized 2,2′(hydrazine-1,2-diylidenebis(propan-1-yl-1-ylidene))diphenol

Tuncay Karakurt [a,*], Alaaddin Cukurovali [b], Nuriye Tuna Subasi [c], Abdurrahman Onaran [d], Abdulilah Ece [e], Sıtkı Eker [f], Ibrahim Kani [g]

[a] Department of Chemical and Process Engineering, Faculty of Engineering-Architecture, Ahi Evran University, Kirsehir 40100, Turkey
[b] Department of Chemistry, Faculty of Science, Firat University, 23119 Elazig, Turkey
[c] Department of Food Engineering, Faculty of Engineering and Architecture, Ahi Evran University, 40100 Kırsehir, Turkey
[d] Department of Plant Protection, Faculty of Agriculture, Gaziosmanpaşa Üniversitesi, 60250 Tokat, Turkey
[e] Department of Pharmaceutical Chemistry, Faculty of Pharmacy, Biruni University, Istanbul 34010, Turkey
[f] Department of Physics, Faculty of Sciences and Letters, Ahi Evran University, 40100 Kirsehir, Turkey
[g] Department of Chemistry, Faculty of Science, Anadolu University, 26470 Eskisehir, Turkey

ARTICLE INFO

Article history:
Received 10 August 2017
In final form 9 January 2018
Available online 11 January 2018

Keywords:
Schiff base, tautomeric forms
AIM
Molecular docking
MM-GBSA

ABSTRACT

In the present study, a single crystal of a Schiff base, 2,2′(hydrazine-1,2-diylidenebis(propan-1-yl-1-ylidene))diphenol, was synthesized. The structure of the synthesized crystal was confirmed by ^{1}H and ^{13}C NMR spectroscopic and X-ray diffraction analysis techniques. Experimental and theoretical studies were carried out on two tautomeric structures. It has been observed that the title compound studied can be in two different tautomeric forms, phenol-imine and keto-amine. Theoretical calculations have been performed to support experimental results. Accordingly, the geometric parameters of the compound were optimized by the density functional theory (DFT) method using the Gaussian 09 and Quantum Espresso (QE) packet program was used for periodic boundary conditions (PBC) studies. Furthermore, the compound was also tested for *in vitro* antifungal activity against *Sclerotinia sclerotiorum, Alternaria solani, Fusarium oxysporum f. sp. lycopersici* and *Monilinia fructigena* plant pathogens. Promising inhibition profiles were observed especially towards *A. solani*. Finally, molecular docking studies and post-docking procedure based on Molecular Mechanics-Generalized Born Surface Area (MM-GBSA) were also carried out to get insight into the compound's binding interactions with the potential. Although theoretical calculations showed that the phenol-imine form was more stable, keto-amine form was predicted to have better binding affinity which was concluded to result from loss of rotational entropy in phenol-imine upon binding. The results obtained here from both experimental and computational methods might serve as a potential lead in the development of novel anti-fungal agents.

1. Introduction

Since Schiff base containing compounds have properties such as antibacterial, anticancer and antioxidant, they are used as starting materials in the synthesis of many pharmaceuticals. In particular, *o*-hydroxy Schiff bases are highly attractive with two different tautomeric structures, which have the intramolecular N—H···O and O—H···N hydrogen bonds, respectively expressed as keto-amine and phenol-imine. These compounds exhibited photochromism and thermochromism properties. The features of photochromism are used in some application areas such as measuring and controlling radiation intensity, imaging systems and optical computers [1]. There are quite wide working areas of Schiff bases. Schiff bases (azomethines, imines) are organic intermediates commonly used for the production of pharmaceutical or rubber additives [2]. Schiff bases are used to determine the amount of metal, but also used in the dye industry due to their transparency, solidity and color. These compounds are used as spectrophotometric reagents in analytical chemistry due to their selective and specific reaction to certain metal ions [3]. Cu(II) complexes formed from Schiff base ligands have been important model compounds in studying the physical and chemical behavior of biological copper systems [4].

* Corresponding author.
E-mail addresses: tuncaykarakurt@gmail.com, tuncay.karakurt@ahievran.edu.tr (T. Karakurt).

https://doi.org/10.1016/j.cplett.2018.01.016
0009-2614/

Thiazole and its derivatives are important in biological systems as antitumor, anti-inflammatory or analgesic agent and as inhibitors of lipoxygenase enzyme [5,6]. Undoubtedly, novel antibiotics are needed because of the resistance of the bacteria to drugs used against infectious diseases. Particularly these compounds can also be found in the composition of fungicides and pesticides. Schiff bases have been used as substrates in the preparation of the vast majority of industrial and bioactive compounds via replacement substitution, ring addition and ring closure reactions [7]. The biological activities of Schiff bases as antitumor, antifungal and herbicide, insecticidal and antibacterial agent are well known.

In the light of the aforementioned critical features, a Schiff base, 2,2′(hydrazine-1,2-diylidenebis(propan-1-yl-1-ylidene))diphenol was synthesized in the current study. The structure of this compound, was confirmed by IR, ^{1}H NMR, ^{13}C NMR and X-ray diffraction analysis techniques. In order to support the experimental studies, theoretically IR and NMR spectra, potential energy distributions (PED) of vibration frequencies, frontier molecular orbitals (FMO) were studied using quantum chemical calculations with 6-311G(d,p) basis set [8] and DFT theory [9,10] using Gaussian 09 software [11]. In addition, the Gausview 5 [12] was used to visualize gaussian outputs.

Quantum Espresso 6.2 [13] package program was used to calculate the total energy per unit cell of the crystal structure by using periodic boundary conditions (PBC).

The antifungal activity tests of the synthesized compound were carried out *in vitro* at four different doses. Finally, molecular docking simulations were also carried out to shed light on the binding modes of both tautomeric forms.

2. Materials and methods

2.1. Determination of X-rays crystal structure

X-ray diffraction data of crystals were collected using MoKα radiation with Bruker AXS APEX CCD [14] diffractometer. The structure solution of the crystals was obtained by direct methods using SHELXT-2014 [15]. In order to determine the locations of atoms other than hydrogen in the solution stage, the SHELXL-2014 [16] using the full matrix least squares method was performed for refining process. In the first stage of the refinement, isotropic treatment was carried out to make atomic positions more sensitive and to identify missing atoms. As a result of the refinement, anisotropic treatment was carried out without adding hydrogen atoms and then the positions of the hydrogen atoms were geometrically determined according to the lapping method. The aromatic C—H bond lengths were fixed as 0.93 Å, the methylene C—H_2 bond lengths were 0.97 Å, and the methyl C—H_3 bond lengths were 0.96 Å, while the hydrogen atoms were geometrically located. Olex2 [17] was used for the structure analysis and refinement calculations, and Mercury 3.9 [18] was used for the molecular drawings.

2.2. Synthesis of the crystal

To a solution of 2′-hydroxypropiophenone (10 mmol) in 50 mL of ethanol together with catalytic amount of *p*-toluene sulfonic acid, a solution of hydrazinium hydroxide (30 mmol) in 20 mL of absolute ethanol was added and refluxed. End of the reaction was determined with IR spectroscopy. Thus obtained substance precipitated with the slow edition of water and crystallized by slow evaporation of its ethanol solution (Scheme 1). Yield: 97%, melting point: 412 K. Characteristic IR bands: 4000–2200 cm^{-1} ν (—OH), 3090 cm^{-1} ν(C—H aromatics), 2980–2874 cm^{-1} ν(aliphatics), 1609 cm^{-1} (C=N azomethine), Characteristic ^{1}H NMR shifts ($CDCl_3$, δ, ppm): 1.36 (t, *j* = 7.8 Hz, 6H, —CH_3), 3.10 (q, *j* = 7.8 Hz, 4H, —CH_2—), 6.99 (td, j_1 = 7.6 Hz, j_2 = 1.2 Hz, 2H, aromatics), 7.08 (dd, j_1 = 8.3 Hz, j_2 = 1.2 Hz, 2H, aromatics), 7.42 (td, j_1 = 8.0 Hz, j_2 = 1.6 Hz, 2H, aromatics), 7.68 (dd, j_1 = 8.0 Hz, j_2 = 1.6 Hz, 2H, aromatics), 13.48 (s, 2H, —OH). Characteristic ^{13}C NMR shifts ($CDCl_3$, δ, ppm): 173.25, 161.20, 132.97, 128.78, 119.09, 118.15, 117.70, 21.64, 11.77.

2.3. Computational details

Crystalline optimize process and some parameters of them were calculated using the Gaussian 09 program with the B3LYP [19,20] method and the 6-311G(d,p) basis set in gas phase. The obtained results were visualized with the help of Gausview 5 program. Potential energy distribution (PED) values for vibration frequencies were calculated using the VEDA 4 [21] program.

All calculations were performed with the QE program at periodic boundary conditions. In these calculations, PWscf (Plane-Wave self-consistent field) program set, one of the main components of quantum espresso and which is based on density functional theory (DFT), plane waves and pseudopotansiyel, was used. For the exchange correlation energy, Local Density Approximation (LDA) which uses of the Perdew-Zunger (PZ) [22] functional was chosen.

Molecular docking studies were performed with the Schrödinger suite 2017-1 [23] program. Some molecular properties such as molecular weight, percent human oral absorption, polar surface area (PSA) and logarithm of octanol-water partition coefficient (QPlogPo/w) were calculated using QikProp module of Schrodinger [24].

2.4. Fungal isolates and effect of the molecule on the antifungal activity of in vitro

In this study, *Sclerotinia sclerotiorum* (isolated from cucumber), *Alternaria solani* (isolated from tomato), *Fusarium oxysporum f.sp. lycopersici* (isolated from tomato), and *Monilinia fructigena* (isolated from apple) plant pathogens were used for the antifungal activity tests. The inoculum of the pathogens was developed on PDA

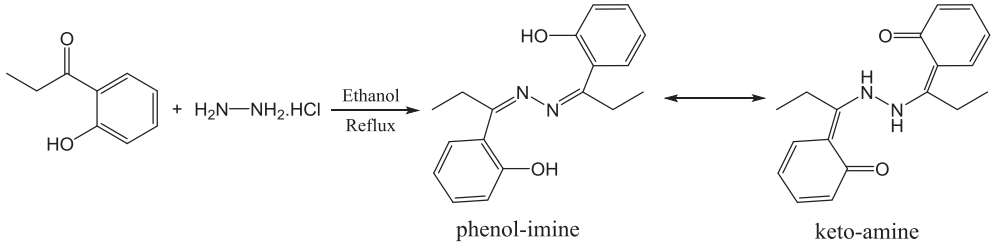

Scheme 1. Synthetic pathway for the synthesis of the target compounds.

(potato dextrose agar) medium for 7 days at 22 ± 2 °C. It was used throughout the study period.

The antifungal activity of the compound in different concentrations was determined by agar plate method [25]. Solutions were added to PDA at 40 °C to give the concentration of 16, 8, 4 and 2 mg/mL for compound and then the PDA with compound was poured (~10 mL/plate^{-1}) each alone in petri plates (60 mm in diameter). Seven-day-old agar discs (5 mm in diameter) bearing the desired fungus growth was transferred into the petri plates. These fungus cultures were incubated at 25 ± 2 °C for 7 days. Fungus growth was recorded daily [26]. Commercial fungicide [Thiram 80% (Hektaş, group)] was used as a positive control. Dimethyl sulfoxide was used as a negative control. Experiment was set up 4 replications and repeated 2 times.

The percentage of mycelial growth inhibition was calculated accordingly the formula given by Pandey et al. [27].

$$I = 100 \times (dc - dt)/dc$$

I; Mycelial growth inhibitiondc; Is the mycelial growth in controldt; Is the mycelial growth in treatment

3. Result and discussion

3.1. Geometrical structure of title compound

The crystal parameters of the $C_{18}H_{20}N_2O_2$ molecule, the details of the data collection and refining process in Table 1, the molecule is drawn with experimental 20% probability ellipsoids in Fig. 1a and the input molecule used in the gaussian program is given in Fig. 1b.

The molecule shown in Fig. 1a consist of a half molecule in the asymmetric unit and is completed by a crystallographic reflection center at 1-x, 1-y, -z. This molecule consists of a Z, Z configuration according to two ethylidene C=N and N1A—N1—C7—C6 torsion angles. The compound has two phenol rings and propane groups which are parallel to each other in the symmetric unit. The angle between the two phenol rings is 0.10 (5)°. The bond length of C1—O1 is experimentally 1.34 (15) Å and in accordance with the literature value of 1.37 (14) [27]. The bond lengths of C7=N1, N1—N1A, C6—C7, C6—C5 and C5—C4 are experimentally 1.29 (3), 1.39 (18), 1.47 (16), 1.40 (16) and 1.37 (2) Å. These lengths are in accordance with literature values 1.2835 (14), 1.3954 (12), 1.4876 (14), 1.3906 (15) and 1.3904 (16) Å [28] and 1.279 (3), 1.406 (3), 1.486 (3), 1.399 (3) and 1.383 (3) Å [29] respectively. The bond lengths of C1—O1 indicating the single bond character and C7=N1 indicating the double bond character support the adoption of the phenol-imine form of the molecule. Looking at the difference in the electron density of the crystal atom H4a in the keto-amine form in the asymmetric unit in Fig. 2a, while the green color shows areas where the electron density is high, the brown-violet nets show holes, and in the keto-amine form, it can be said that the atom H4a is in the wrong position. In Fig. 2b we can also say that the atom H4a in the crystal in phenol-imine form is correctly positioned.

An intramolecular O—H···N bond was observed in the crystal. In the crystal, there is no classical hydrogen bond between molecules and inter-molecular π- π interactions and van der Waals interactions are observed in the structure. Molecules are connected to each other by these interactions. The molecular structure is adopted to form the phenol-imine form and it has become stable with O—H···N-type intramolecular hydrogen bond by forming the S (6) closed ring.[1] Symmetry operation operators, which supply the crystal in phenol-imine form to repeat itself in 3-D space, are shown in Fig. 3 (yellow circle = inversion, purple line = slip plane, green line = 2-axis screw symmetry processors).

Table 1
Data collection and refinement values of $C_{18}H_{20}N_2O_2$ crystal.

Crystal form	Phenol-imine form
Empirical formula	$C_{18}H_{20}N_2O_2$
Formula weight	148.18
Temperature/K	296.15
Crystal system	Monoclinic
Space group	$P2_1/n$
a/Å	7.6062(7)
b/Å	6.5754(6)
c/Å	15.8462(13)
α/°	90
β/°	96.447(4)
γ/°	90
Volume/Å^3	787.52(12)
Z	2
ρ_{calc}g/cm^3	1.250
μ/mm^{-1}	0.082
F(0 0 0)	316.0
Crystal size/mm^3	0.3 × 0.1 × 0.09
Radiation	MoKα (λ = 0.71073)
2Θ range for data collection/°	5.174 to 56.606
Index ranges	$-10 \le h \le 9$, $-8 \le k \le 8$, $-20 \le l \le 20$
Reflection collected	6739
Independent reflections	1879 [R_{int} = 0.0205, R_{sigma} = 0.0200]
Data/restraints//parameters	1879/0/105
Goodness-of-fit on F^2	1.074
Final R indexes [I ≥ 2σ (I)]	R_1 = 0.0440, wR_2 = 0.1143
Final R indexes [all data]	R_1 = 0.0627, wR_2 = 0.1262
Largest diff. peak/hole/e Å^{-3}	0.17/−0.18
CCDC	1,563,361

At the end of the solution process, the drawing of the molecules belonging to phenol-imine form with the π- π interactions in the unit cell is shown in Fig. 4, the information about the hydrogen bond is given in Table 2.

The experimental results for the phenol-imine form and the bond lengths and bond angles of the theoretical calculation results for both forms are listed comparatively in Table 3.

3.2. Tautomerism

We have studied with the theoretical calculations that two tautomer structures such as phenol-imine and keto-amine were occurred or not in the asymmetric unit in the molecule we have worked on. Two tautomeric structures and some structural parameters of the transition state of the molecule were calculated theoretically using DFT/B3LYP method with 6-311G(d,p) base-set. The energies of the two tautomeric structures and the differences between them and also the activation energies of forward and backward reactions were shown in Table 4. The imaging frequency of the transition state of the molecule is calculated as 724 cm^{-1} and thus the correctness of the transition state is proven.

Phenol-imine and keto-amine tautomeric forms can be converted into each other by an intramolecular proton transfer reaction. Some changes may occur in the structure due to the migration of the hydrogen atom from the O atom to the N atom or from the N atom to the O atom. While the proton transfer from the phenol-imine form to the keto-amine form takes place the O—H bond length is increased and broken. The broken H atom from the oxygen atom bonds to the N atom and the proton transfer process is completed. As shown in Table 3, when this process takes place, the N1—C7, C5—C6 and C1—C2 bond lengths and the N1—C7—C6 bond angle increased while the O1—C1, C6—C7 bond lengths and the O1—C1—C6 bond angle decreased. From a structural point of view, all results show that the transition state is more

[1] For interpretation of color in Figs. 3 and 13, the reader is referred to the web version of this article.

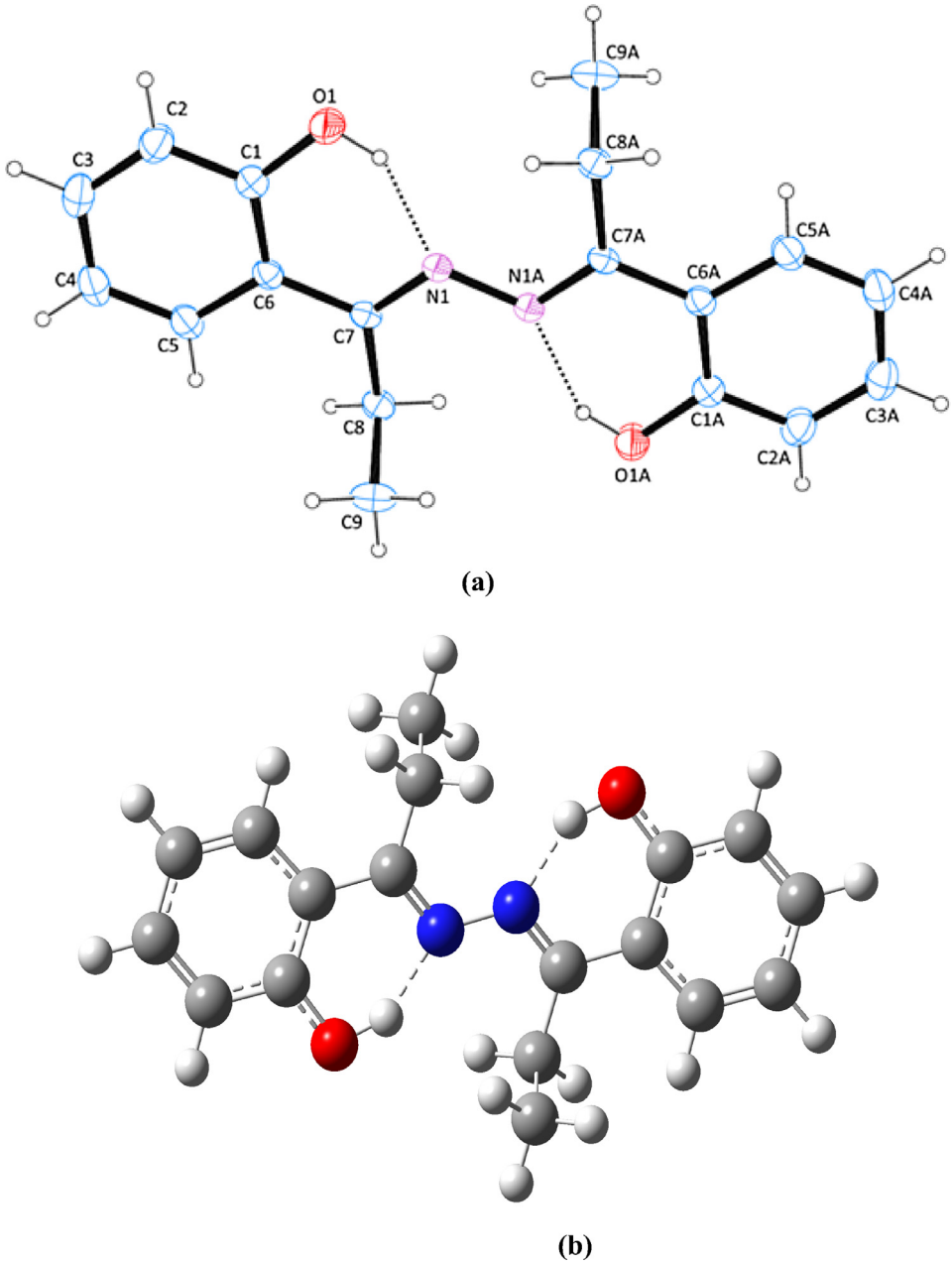

Fig. 1. The phenol–imine form of $C_{18}H_{20}N_2O_2$ crystal (a) experimental (b) calculated shapes.

similar to the phenol-imine form than the keto-amine form and the transferred proton is closer to the phenol-imine form rather than keto-amine form.

The energy profile of the proton transfer process is shown in Fig. 5. This energy is calculated as the difference between the two forms and TS. This energy difference is calculated as −5.24 kJ/-mol for the gas phase. As seen in Fig. 5, the phenol-imine form is more stable than the keto-amine form. Relative energy of TS in the form of phenol-imine was 36.04 kJ/mol in the gas phase while the back-reaction barrier energy was calculated as 41.28 kJ/mol. These values indicate that there is a significant high energy required for the forward and reverse proton transfer to take place. As a result, it can be said that the reaction of proton transfer on both sides will not be easy. Standard enthalpy and free energy changes in proton transfer are listed in Table 4. As shown in the table, the positive enthalpy and free energy changes in the gas phase during the forward and backward proton transfer show that the two-way reaction is endothermic and that these two reactions cannot take place spontaneously.

3.3. Periodic boundary calculations

The crystal data of the experimental phenol-imine and keto-amine structures belonging to the $P2_1/n$ symmetry group used for QE calculation as the initial set. The simulation cell where the periodic boundary conditions are used contains 84 atoms (Fig. 6).

The total energy corresponding to the cutoff energy (E_{cut}) values is calculated in order to identify the working system in the Plane-Wave self-consistent field program and to determine the most suitable cutoff energy for the modeled system. In the calculations, the lattice constant and k-point set in the system were kept constant in the value of a = 14.373 a.u. and ($2 \times 2 \times 2$). The change of total energy according to E_{cut} is shown in Fig. 7.

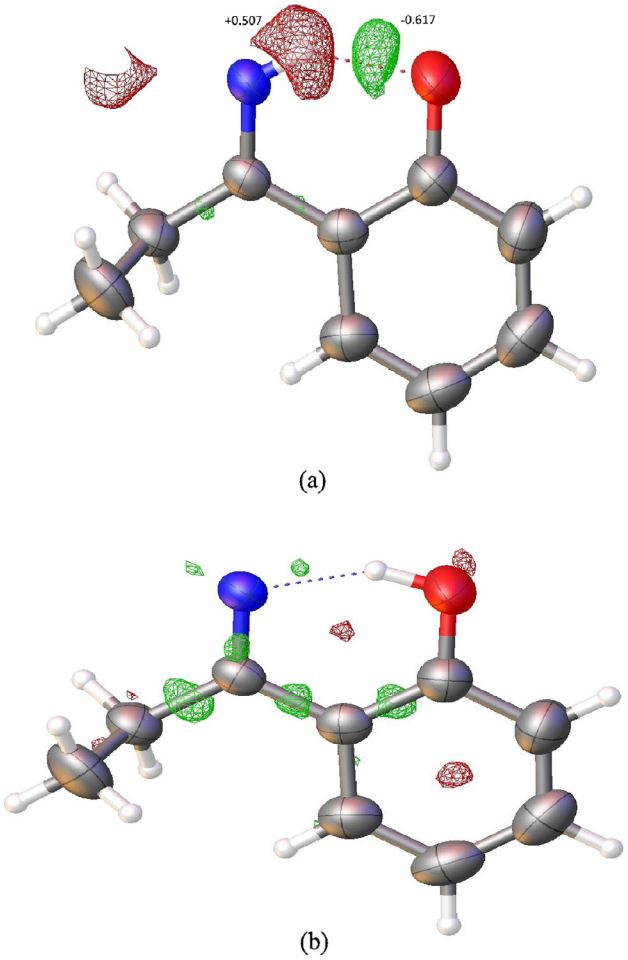

Fig. 2. An early refinement state of title compound showing difference electron density. Missing (green) and erroneously (red) placed H atoms are clearly visible. (For interpretation of the references to color in this figure legend, the reader is referred to the web version of this article.)

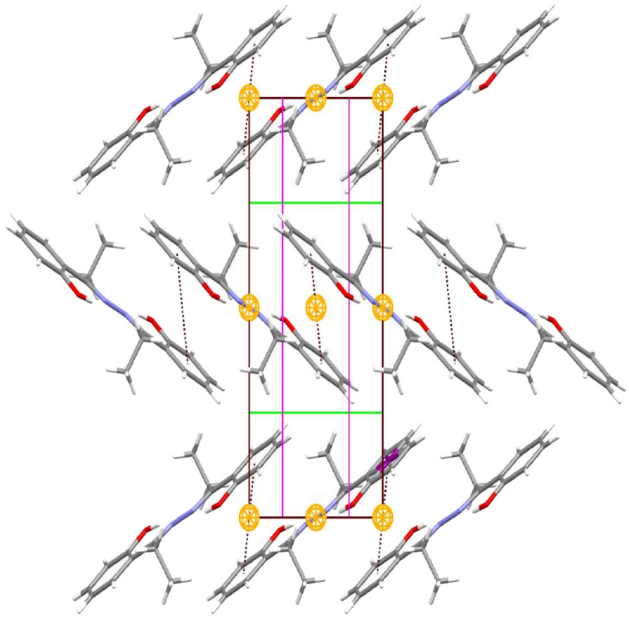

Fig. 3. $C_{18}H_{20}N_2O_2$ crystalline repetition itself with symmetry axes in phenol-imine form.

As can be seen in Fig. 7, the total energy values obtained for the next values of 30 Rydberg (Ry) converge to each other and the total energy values reach constant values after E_{cut} = 30 Ry. In other words, the system has minimum total energy in these values. As a result, it has been seen that increasing the E_{cut} value does not cause a significant change in the total energy of the system. Taking this convergence into consideration, we have taken kinetic energy cutoff value = 65 Ry, as we have seen in the previous published article [30]. For more confidence in the results, a high convergence of 10^{-8} Ry was used on energy. Using the Pwscf'scf (self-consistent field method) option of both forms, we obtained the total energy values per unit cell. The total energy values per unit cell of phenol-imin and keto-amin forms were calculated as −958.74452640 and −958.28637977 Ry, respectively. In this case, it can be said that the phenol-imin form has a more stable structure than the keto-amin form in periodic boundary conditions.

3.4. IR studies

The IR spectrum measured in the range of 4000–400 cm^{-1} is shown in Fig. 8. The molecular symmetric unit has C1 point symmetry containing 42 atoms and has 120 basis vibration frequency, all calculations for vibration frequencies were made for the phenol-imine structure using the DFT (B3LYP/6-311G(d, p)) basis set. Later, the detailed naming of these vibration modes was also done by PED analysis. Experimental and calculated spectra are shown in Fig. 8. It is known that DFT calculations are made in the gas environment. Each frequency value is multiplied by the scale value of 0.9688 [31] to approximate the calculation results to the experimental results. The free vibration frequency of the O—H group, which did not make intramolecular or intermolecular hydrogen bond, peaked between 3550 and 3700 cm^{-1} [1], the bonding group frequency is observed between 3550 and 3200 cm^{-1}[1,32]. In our study, this peak was not observed experimentally because the O—H bond was used in the intramolecular bond, causing the spectrum to be observed to be too broad.

In the theoretical calculations, it was calculated that this vibration frequency is a pure O—H stretching vibration with a PED contribution of 44–40% at 3032–3021 cm^{-1}. In the case of N—H or O—H groups forming intermolecular or intramolecular hydrogen bonds in the molecule, when the stretching vibration frequency values of these groups are decreased bending vibration frequency values are increased [33]. The in-plane angle bending vibration frequency of the O—H mode is experimentally observed to be 1494 cm^{-1}, and in the literature, this frequency is reported as 1392 cm^{-1} [34] and 1409 [35] cm^{-1}. This vibration mode was theoretically calculated to be a pure O—H in-plane angle bending vibration frequency with 13–11% PED contribution at 1616–1491 cm^{-1}. The O—H mode out-of-plane angle bending vibration frequency was experimentally observed at 760 cm^{-1} and was calculated to be a pure O—H out-of-plane angle bending vibration frequency at 425–844 cm^{-1} with 42% PED contribution. In the light of all these results it can be of the opinion that the OH group is used for intermolecular bonding.

N—N and C=N (hydrazone) vibrational frequencies of the other groups were observed experimentally as 1227 and 1609 cm^{-1}, respectively, and the C=N (hydrazone) vibration frequency is in accordance with the literature value [36]. In the calculations made, these peaks were calculated to be a pure N—N vibration frequency at 1156 cm^{-1} with 10% PED contribution and a pure C=N vibration frequency at 1549 cm^{-1} with 24% PED contribution.

In aromatic compounds, the characteristic CH vibration frequency values are observed at 3100–3000 cm^{-1} in the IR spectrum [37], while the C—C aromatic stretching vibration is observed at 1600–1400 cm^{-1} [38]. The C—H and C—C vibrational frequencies in the aromatic rings were experimentally observed between

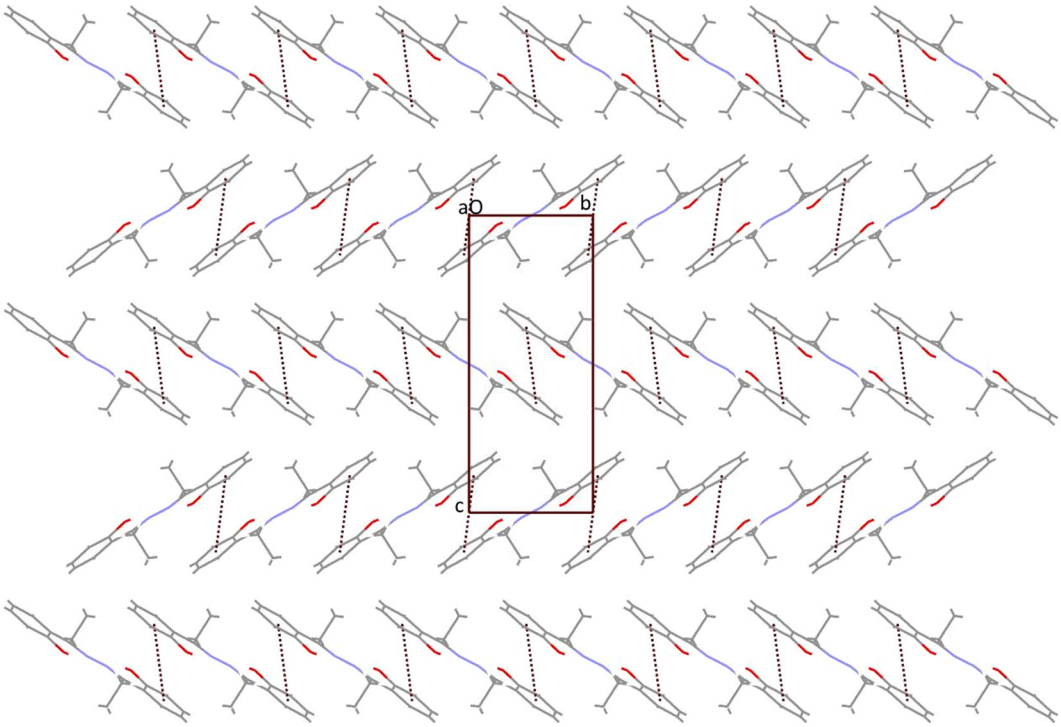

Fig. 4. Packing of the crystal in phenol-imine form with π-π interactions along the c axis.

Table 2
Hydrogen bond geometry for the crystal in phenol-imine form (Å, °).

D—H···A	D—H	H···A	D···A	D—H···A
O1—H1···N1	0.82(2)	1.93(2)	2.65(3)	146(2)

3090 and 1609–1549 cm^{-1}, respectively and the literature values are in accordance with 3110–3003 and 1666–1535 cm^{-1} [39], respectively. The in-plane CH angle bending vibrational frequencies in the aromatic ring are experimentally observed between 1400 and 1000 cm^{-1} [40]. Experimentally, this vibration frequency was observed at 1162–1125 cm^{-1}, theoretically it was calculated as 1155–1072 cm^{-1}. In most hydrocarbons, CH_2 symmetric stretching vibrations occur at 2900–2850 cm^{-1}, while asymmetric stretching vibrations are observed at 3000–2900 cm^{-1} [37]. In this study, the symmetric and asymmetric CH_2 stretching vibrations were observed experimentally at 2874 cm^{-1} and 2980 cm^{-1}, respectively, and theoretically these vibration modes were calculated between at 2980–2943 cm^{-1} and 3033–2999 cm^{-1}.

Table 3
The calculated and experimental geometric parameters of the phenol-imine form of crystal.

Bond lengths (Å)	Experimental (phenol–imine)	DFT (phenol–imine)	DFT (keto-amine)
C1—C2	1.39(18)	1.40	1.51
C1—O1	1.34(15)	1.34	1.25
C2—C3	1.36(2)	1.38	1.54
C3—C4	1.38(2)	1.40	1.55
C4—C5	1.37(2)	1.38	1.54
C5—C6	1.40(16)	1.41	1.52
C6—C7	1.47(16)	1.47	1.40
C7—N1	1.29(14)	1.31	1.35
N1—N1A	1.39(18)	1.38	1.37
C7—C8	1.51(14)	1.51	1.51
C8—C9	1.51(19)	1.54	1.54
Bond Angles (°)			
C1—C2—C3	120.95(13)	120.76	111.99
C3—C4—C5	119.50(13)	119.42	112.82
C4—C5—C6	122.36(13)	122.22	111.35
C6—C7—N1	116.32(9)	116.98	118.03
C7—N1—N1A	116.14(10)	117.01	124.53
O1—C1—C6	122.12(10)	122.59	124.76
C7—C8—C9	113.06(10)	112.84	113.18
Torsion Angles (°)			
C1—C2—C3—C4	0.6(2)	−0.10	−46.43
C3—C2—C1—O1	−179.85(13)	−179.54	−130.87
N1—C7—C6—C1	−5.13(16)	5.42	1.79
C6—C7—N1—N1A	−179.01(11)	178.91	179.66
N1A—N1—C7—C8	0.27(17)	−0.46	0.42

3.5. NMR studies

The ^1H and ^{13}C NMR (see Figs. 9a and 9b) spectra were recorded on a Varian-Gemini 400 MHz spectrometer using tetramethylsilane (TMS) as the internal reference. The GIAO (Gauge-Independent Atomic Orbital) [41,42] method was used to determine the NMR chemical shifts values of the molecules and TMS [tetramethylsilane, $Si(CH_3)_4$] was taken as reference. The ^1H and ^{13}C NMR chemical shift values calculated by selecting chloroform ($CDCl_3$) as solvent for TMS are 31.30 and 175.58 ppm for DFT/B3LYP/6-311G(d,p), respectively. The theoretical ^1H and ^{13}C NMR chemical shift values obtained from by using experimental and optimize structures of the molecule are given in Table 5. When the ^{13}C NMR spectrum is examined, the evidence that the molecule has N and O atoms will be the peaks of C7 and C1 atoms. The chemical shift values of these atoms are higher than those of other carbon atoms. Especially the electronegative atoms (N1 and O1) around the C7 and C1 atoms, due to the high shielding effect around these atoms are caused to resonance at the low field and the chemical shift is experimentally 173.25 and 161.20 ppm, which is greater than that of other carbon atoms. These two chemical shift values were calculated as 180.04 and 169.05 ppm.

The C8 and C9 atoms in the molecule were shifted to resonate at higher field due to hydrogen atoms, which had less shielding effect

Table 4
Energies of the keto–amine and phenol–imine forms of the title compound in hartrees, and energy differences, activation energies, and thermodynamic parameters in kJ mol^{-1}.

phenol–imine	keto-amine	Δ E	Ea(f)	Ea(r)	Δ H298(f)	Δ G298(f)	TΔ S298(f)	Δ H298(r)	Δ G298(r)	TΔ S298(r)
−479.038606	−479.036609	−5.24	36.04	41.28	29.01	32.52	−3.51	23.20	29.54	6.34

Δ E = Eketo-Eenol, Ea(f) = forward activation energy, Ea(r) = reverse activation energy.

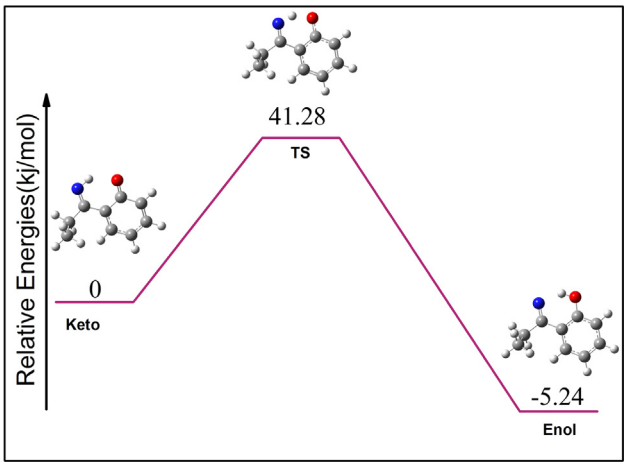

Fig. 5. Potential energy diagram for the direct phenol–imine – keto–amine tautomerism of the title compound (asymmetric unit).

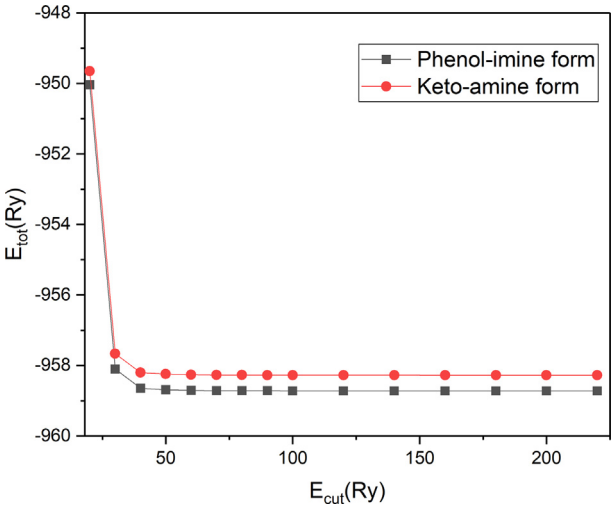

Fig. 7. Change of total energy according to cutting energy of phenol–imine and keto–amine forms.

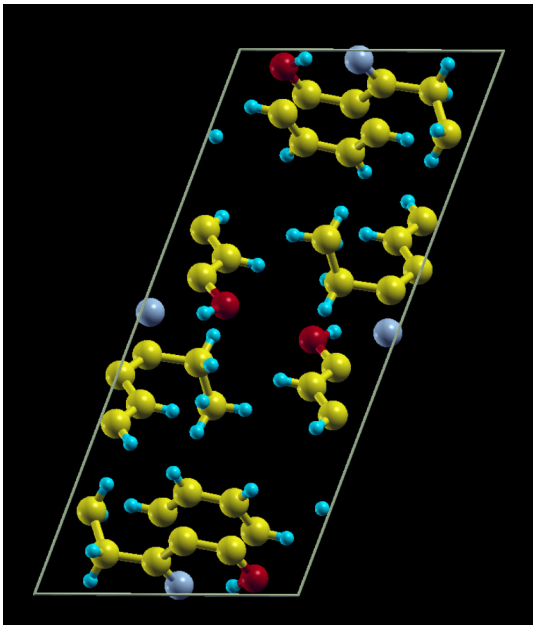

Fig. 6. The atoms within the unit cell of phenol–imine form.

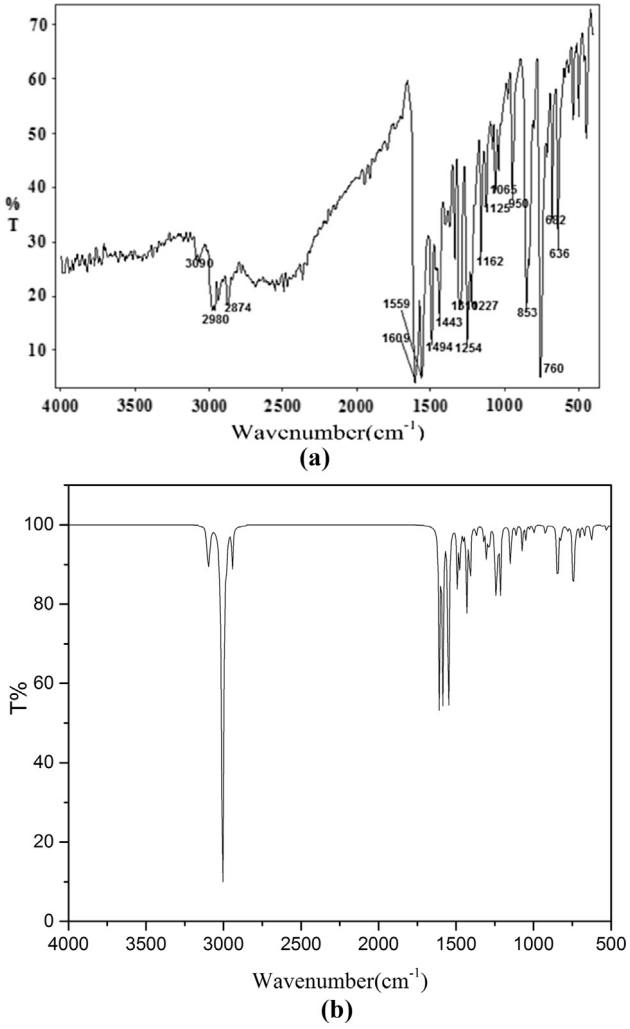

Fig. 8. (a) Experimental (b) Theoretical IR spectrum of the crystals.

than carbon atoms, resulting in less chemical shifts and these peaks were experimentally observed as 21.64 and 11.77 ppm respectively, they were calculated theoretically as 23.87 and 11.66 ppm, respectively. In the ^{1}H NMR spectrum, the hydrogen peak of the hydroxy group was experimentally observed at 13.48 ppm, and in the theoretical calculation, this peak value was calculated as 13.12 ppm. The other peaks of the molecule are given in Table 5.

3.6. Frontier molecular orbitals and molecular hardness

After obtaining stable structure and structural parameters of the title molecule, HOMO and LUMO energy values were investigated.

The most important orbitals in a molecule are the boundary molecular orbitals called HOMO and LUMO. These orbitals describe intramolecular interactions. The HOMO energy determines the electron donating affinity and the LUMO energy determines the electron withdrawing affinity. The energy difference between these two orbitals is a measure of the chemical stability of the molecule and it is a critical parameter in determining the molecular electrical transport properties since it is a measure of the electron conductivity. Therefore this energy difference is largely responsible for the chemical and spectroscopic properties of the molecules [43].

The calculations were carried out in the gas phase and the energy values of HOMO and LUMO in the phenol-imine form of the molecule were −5.92 and −2.29 eV, respectively, while these energy levels in the keto-amine form were −4.98 eV ve −1.40 eV, respectively. As shown in Fig. 10, the ring, phenol-imine and amine groups of the molecule are localized on the HOMO and LUMO orbitals. Electron density and FMO orbital (HOMO and LUMO) energies are very important to explain the molecular properties and biological activities. From a functional point of view, ligands with higher electron transfer capacity interact better with the target protein structure as a result it can be easier to hold on and binding protein. The molecular mechanism of the ligand binding area is described at the quantum chemical level as follows: The HOMO orbitals on the nucleophilic molecule (drug) interact with the LUMO orbitals on the electrophilic agent (enzyme active site) [44].

3.7. Aim analysis

Bader's QTAIM theory is used for more information about the nature of the intermolecular and intramolecular hydrogen bonds in the molecule and the details about its power. The strength of a chemical bond is obtained by using the electron density (ρ_{BCP}) at BCP [45]. Knowing the value of bond at a bond critical point (ρ_{BCP}) is almost like knowing that bond is occurred with what kind of interaction. The Laplacian of the electron density of the critical points in the BCP is shown by $\nabla^2(\rho_{BCP})$, and this value is negative in the covalent bonds. However, in the case of bonds formed by ionic, Van der Waals and hydrogen interactions, $\nabla^2(\rho_{BCP}) > 0$ due to the decrease of electron density in BCP. The presence of the hydrogen bond, according to QTAIM theory, can be classified according to Rozas et al. [46] as follows: (i) The strong hydrogen bonds in the covalent character are characterized by $\nabla^2(\rho_{BCP}) < 0 and\ HBCP < 0$. (ii) Moderate hydrogen bonds with partial-covalent character are characterized by $\nabla^2(\rho_{BCP}) > 0$ and $H_{BCP} < 0$. (iii) Weak hydrogen bonds in the electrostatic character are characterized by $\nabla^2(\rho_{BCP}) > 0$ and HBCP > 0 and the distance between the interacting atoms is larger than Van der-Waal's radius. The H_{BCP} here is the total electron energy density at the critical bond point. Molecular graphs of structures using the AIMAII [47] program are shown in Fig. 11.

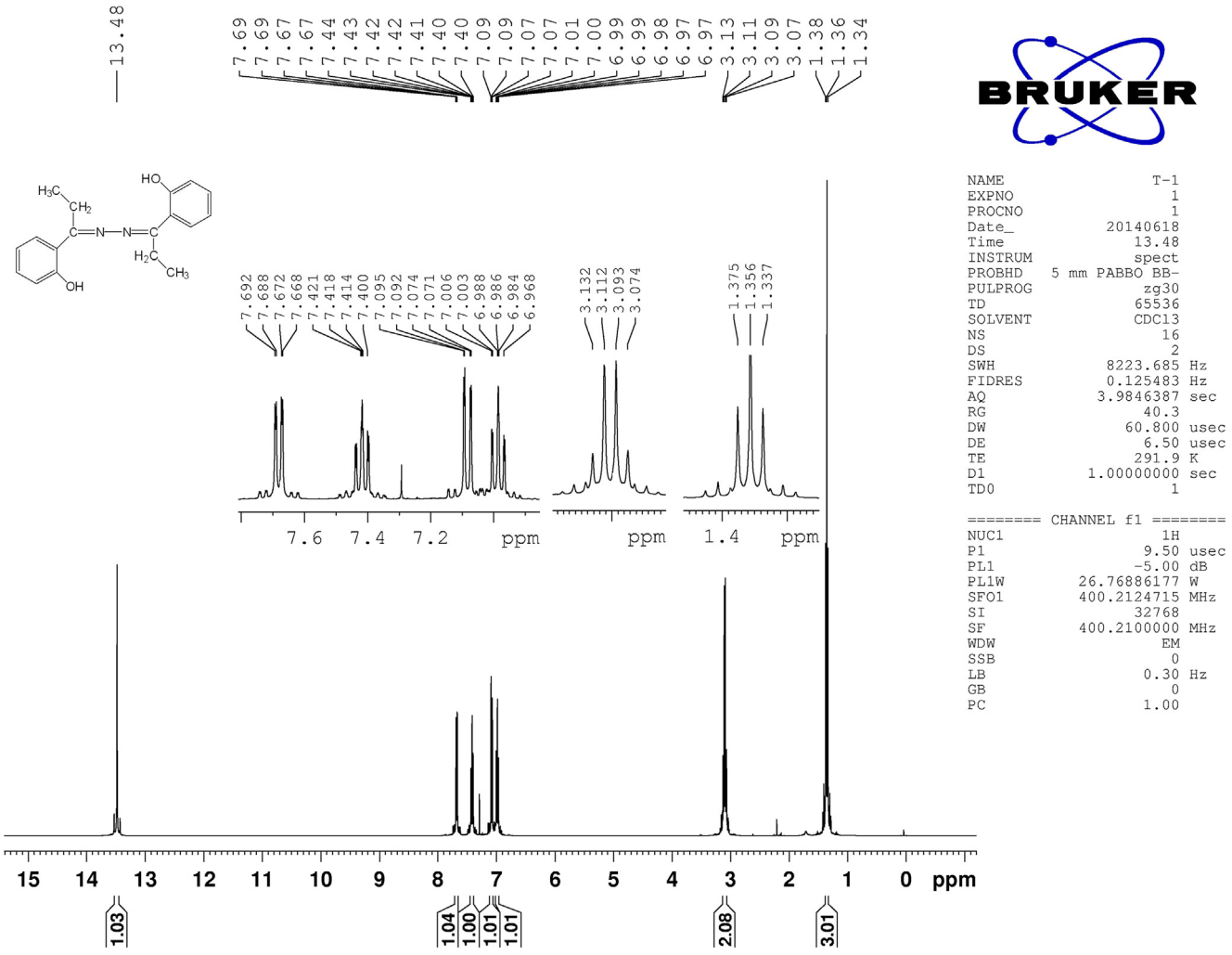

Fig. 9a. ^{1}H NMR spectrum of target compound.

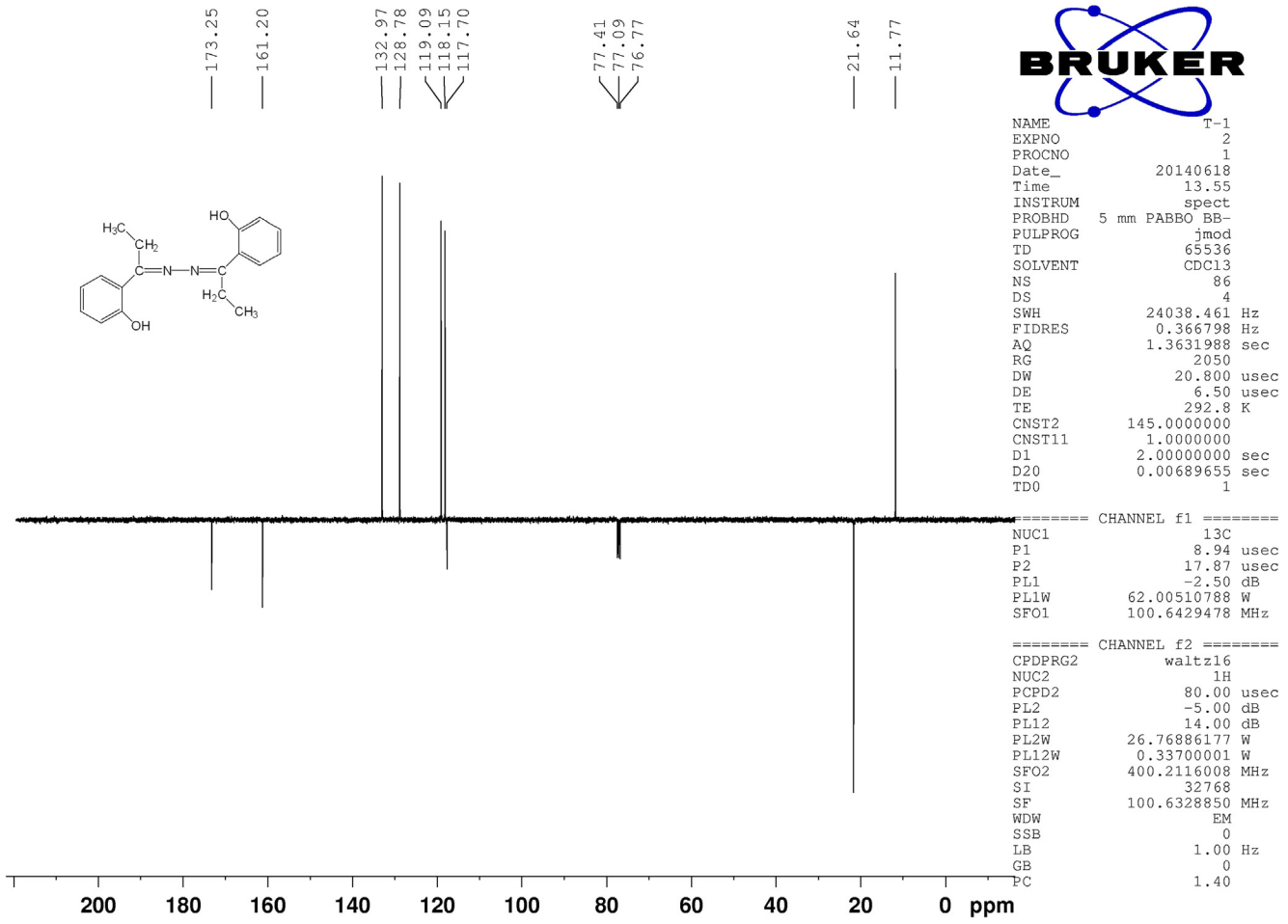

Fig. 9b. ^{13}C NMR spectrum (APT technique) of target compound.

Table 5
Theoretical ^{1}H and ^{13}C isotropic chemical shift values of molecule (with respect to TMS, all values in ppm).

Atom	Experimental	DFT (phenol–imine)	DFT (keto–amine)
C1	161.20	169.05	198.36
C2	117.70	121.22	124.12
C3	132.97	137.37	136.14
C4	118.15	121.31	151.79
C5	128.78	133.36	134.62
C6	119.09	121.66	105.45
C7	173.25	180.04	183.39
C8	21.64	23.87	36.13
C9	11.77	11.66	13.74
H(OH)	13.48	13.12	–
H(CH) (benzene ring)	6.99–7.68	7.01–7.80	5.96–7.64
H (CH2)	3.10	2.83–3.21	2.36–3.00
$H(CH_3)$	1.36	1.12–1.31	1.05–1.22

The topological parameters for the bonds of the atoms that interact at the critical bond point (BCP) are given in Table 6. Various types of interactions observed in molecular graphics are classified according to geometric, topological and energetic parameters. In this work, the Bader's theory was also used to calculate hydrogen bond energy. Espinosa suggested the relationship between the hydrogen bond interaction energy and the potential energy density as $E_{int} = 1/2(V_{BCP})$ [48]. As seen in Table 6, the value of H_{BCP} in the interaction of the hydrogen bond in the form of phenol-imine (O—H···N) is negative, whereas it is positive in the form of keto-amine (N—H···O). According to the criterias ii. and iii. given by Rozas and his colleagues the hydrogen bond in the phenol-imine form was stronger. Again according to the aim calculations, the E_{int} energy of the phenol-imine form is calculated smaller than the keto-amine form.

3.8. Biological activity

Antifungal activity values (Mycelial growth and Mycelial growth inhibition) of the Schiff-based molecule used against *Sclerotinia sclerotiorum, Alternaria solani, Fusarium oxysporum f.sp. lycopersici* (FOL) and *Monilinia fructigena* are presented in Table 7.

The Schiff-base molecule used against plant diseases showed antifungal activity at varying rates. For the four different doses used in the molecule, as the dose increases the value of antifungal activity has shown an increase. The Schiff-base molecule used at doses of 16, 8, 4 and 2 mg/mL, mycelial growth inhibition were observed at between 43.2 and 69.2% against *S. sclerotirum*, between 16.3 and 60.5% against *A. Solani,* between 11,7 and 41,2% against Fol and between 9.8 and 38.3% against *M. Fructigena*. When considering the obtained antifungal activity values, it was determined that *S. sclerotiorum, A.solani,* FOL and *M. Fructigena* fungus species were the least affected towards most affected, respectively. Commercially available thiram 80% which has been used at the proposed commercial dose of the company inhibition was observed in the ratio of 100% against *S. Sclerotiorum*, 69,7% against *A.solani*, 68,7% against FOL and 62,8% *M. Fructigena*. Antifungal activity was not observed in DMSO used as a negative control. Based on

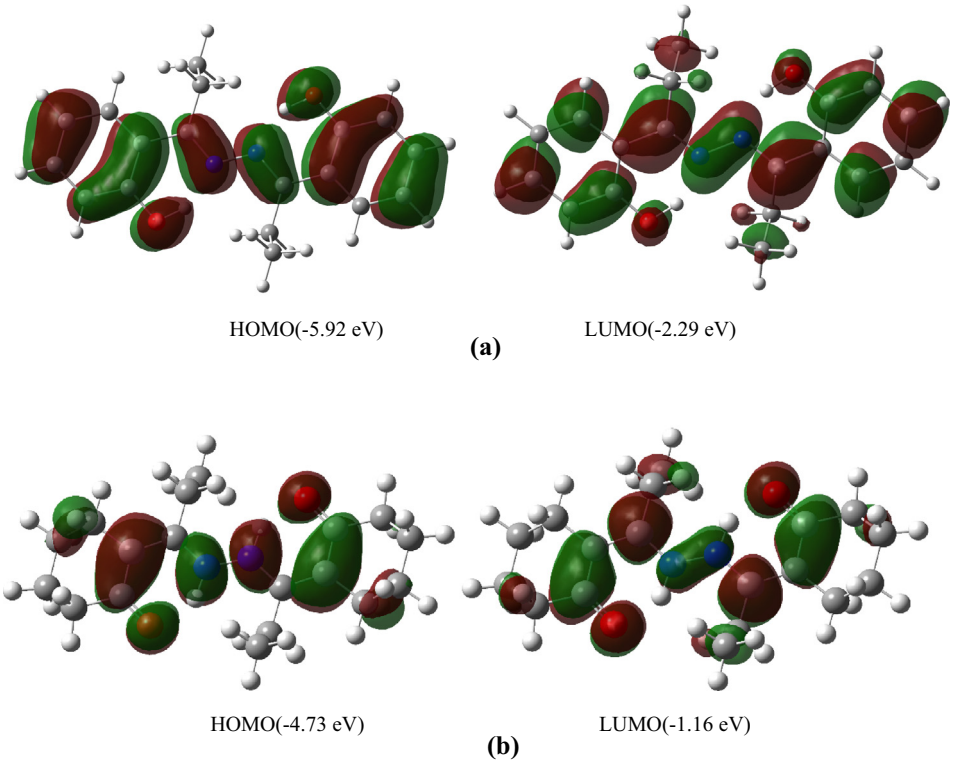

Fig. 10. Crystalline (a) phenol–imine (b) keto–amine Frontier orbitals and energies.

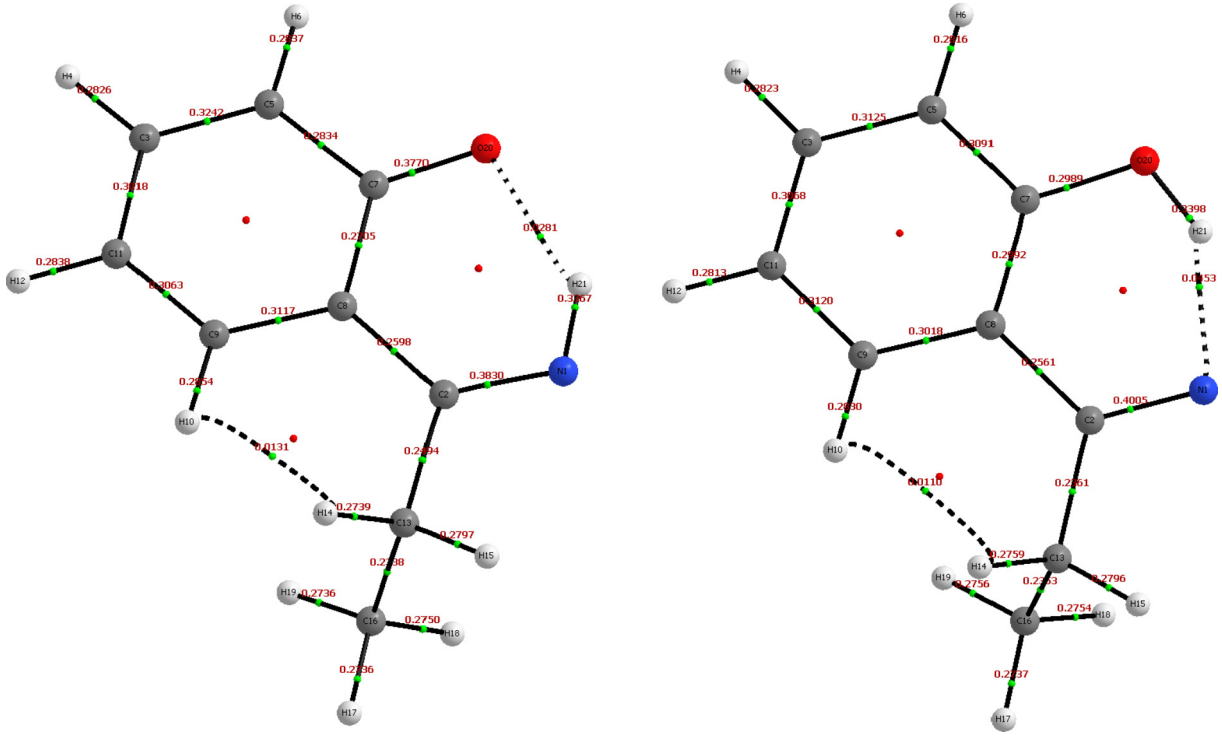

Fig. 11. Molecular graph of phenol–imine and keto–amine forms: bond critical points (small green spheres), ring critical points (small red spheres). (For interpretation of the references to color in this figure legend, the reader is referred to the web version of this article.)

these results, it was determined that the Schiff-base molecule showed high-middle and low levels of antifungal activity against the pathogens used in our study and promising results were obtained.

3.9. Molecular docking studies

A high resolution (1.6 Å) X-ray crystal structure of trichothecene 3-O-acetyltransferasein complexed with Coenzyme A

Table 6
Topological parameters for bonds of interacting atoms: electron density (ρ_{BCP}), Laplacian of electron density ($\nabla^2\rho_{BCP}$), kinetic electron energy density (G_{BCP}), potential electron energy density (V_{BCP}), total electron energy density (H_{BCP}), estimated interaction energy (E_{int}) at bond critical point (BCP).

Interaction	ρ_{BCP} (a.u.)	$\nabla^2\rho_{BCP}$ (a.u.)	G_{BCP} (a.u.)	V_{BCP} (a.u.)	H_{BCP} (a.u.)	E_{int} (kcal/mol)
Phenol–imine (O—H···N)	0.0453	0.1121	0.0344	−0.0407	**−0.0063**	−12.7696
Keto–amine (N—H···O)	0.0281	0.1000	0.0234	−0.0218	**+0.0016**	−6.8398

Table 7
Antifungal activity values (MG and MGI) against plant pathogenic fungi of Schiff-based molecule.

Doses mg/mL	Plant pathogenic fungi							
	S. sclerotiorum		*A. solani*		*FOL*		*M. fructigena*	
	MG (mm)	*MGI* (%)	MG (mm)	*MGI* (%)	MG (mm)	*MGI* (%)	MG (mm)	*MGI* (%)
16 mg/mL	18,5	*69,2*	22,3	*60,5*	35,3	*41,2*	*28,2*	*38,3*
8 mg/mL	24,2	*59,7*	38,6	*31,7*	43,7	*27,2*	*33,7*	*26,3*
4 mg/mL	28,1	*53,2*	40,4	*28,5*	46,9	*21,8*	*37,4*	*18,2*
2 mg/ml	34,1	*43,2*	47,3	*16,3*	53,0	*11,7*	*41,2*	*9,8*
C+ (Thiram)	0,0	***100***	17,1	***69,7***	**18,8**	***68,7***	***17,0***	***62,8***
C− (DMSO)	60,0	*0,0*	56,5	*0,0*	60,0	*0,0*	*45,7*	*0,0*

MG = Mycelial growth, MGI: Mycelial growth inhibition, C+: Positive control; C−: Negative control.

Table 8
Docking scores and selected molecular properties of phenol–imine - keto–amine forms and the native ligand, ZBA.

Compound	Dscore (kcal/mol)	MMGBSAdG Bind (kcal/mol)	E HOMO (eV)	MW[a] (g/mol)	%Human oral absorption[b]	PSA[c] Å^2	QPlogPo/w[d]	Rule of five
ZBA	−7.939	−62.20	−6.80	464.511	91.572	137.570	2.475	+
keto–amine **form**	−5.713	−41.88	−4.73	296.368	100.000	70.225	4.020	+
phenol–imine **form**	−4.514	−29.62	−5.92	296.368	100.000	56.646	3.596	+

[a] Molecular weight (recommended value <5 0 0).
[b] Percentage of human oral absorption (<25% is weak and >80% is strong).
[c] Polar surface area (recommended value $\leq$ 140 Å^2) [58].
[d] Logarithm of the partition coefficient of the compound between n-octanol and water (recommended value < 5).

and T-2 mycotoxin (ZBA) was downloaded from protein data bank (PDB ID: 2RKV) and prepared using the Protein Preparation Wizard (PrepWizard) in Maestro of Schrödinger software package [49].

As an initial step, all hydrogen atoms were added to the raw structure and any water and heteroatoms except native ligand (ZBA) were removed in the PrepWizard. The missing side chains were also added and bond orders were assigned. Then the structure was optimized at neutral pH. This helps to remove the steric clashes between the atoms. Energy minimization was then carried out using default constraint of 0.3 Å RMSD and OPLS3 force field [50].

Glide SP (standard precision) module of Schrödinger Suite [51,52] was used for docking calculations. The binding pocket was defined by generating a grid which is a cubic box of specific dimensions centered on the centroid of the native ligand. The default parameters were kept. A post-docking procedure based on Prime's Molecular Mechanics-Generalized Born Surface Area (MM-GBSA) [53–55] protocol using VSGB solvation model [56] was also performed.

We have calculated some molecular descriptors commonly used in absorption, distribution, metabolism and excretion (ADME) analysis and number of violations of Lipinski's rule of five which is an indication of the drug-likeness of a molecule [57] were also estimated (Table 8). As can be seen from Table 8 all compounds including the native ligand **ZBA** obey Lipinski's rule of five.

On the other hand, molecular docking is a value added computational tool used in computer aided drug design to sample ligand poses in the binding pocket and analyze the intermolecular interactions with the target macromolecule [59–63]. We employed molecular docking simulations in order to explore the structural–functional inhibition mechanism. Before going further, we docked the native ligand ZBA and the resulting binding mode was in agreement with the crystal structure yielding a RDMD value of 0.897. As can be seen from Fig. 12, the native ligand ZBA makes hydrogen bond contacts with the Tyrosine 413 and Histidine 156 of the target enzyme.

The docking studies revealed that the keto–amine form has both higher docking score and also better binding free energy obtained by a more superior MM/GBSA method than the phenol–imine form and it has similar binding interactions with ZBA (Fig. 13a–b). Keto–amine form binds to a narrow hydrophobic pocket. Although it does not make hydrogen bond with HIS 156, the carbonyl oxygen of the keto–amine form participates in the formation of a critical hydrogen bonding with the Tyrosine 413 by acting as a hydrogen bond acceptor. Hence, the carbonyl group might be a vital moiety in enhancing the interactions with the target.

The binding surfaces of the target together with ZBA, keto-amine and phenol-imine forms were produced and colored with electrostatic potential map (Fig. 13). The red color shows areas of high electron density and the blue color shows areas of low electron density. The keto-amine form seems to be well fitted in the binding cavity and it also has positive electrostatic interactions with the target. The low electron density region of the ligand interacts with the high electron density region of the active site. On the other hand, unfavorable interactions in case of phenol-imine can be observed since its binding conformation is different from ZBA and phenol–imine form (Fig. 14). Furthermore, phenol group

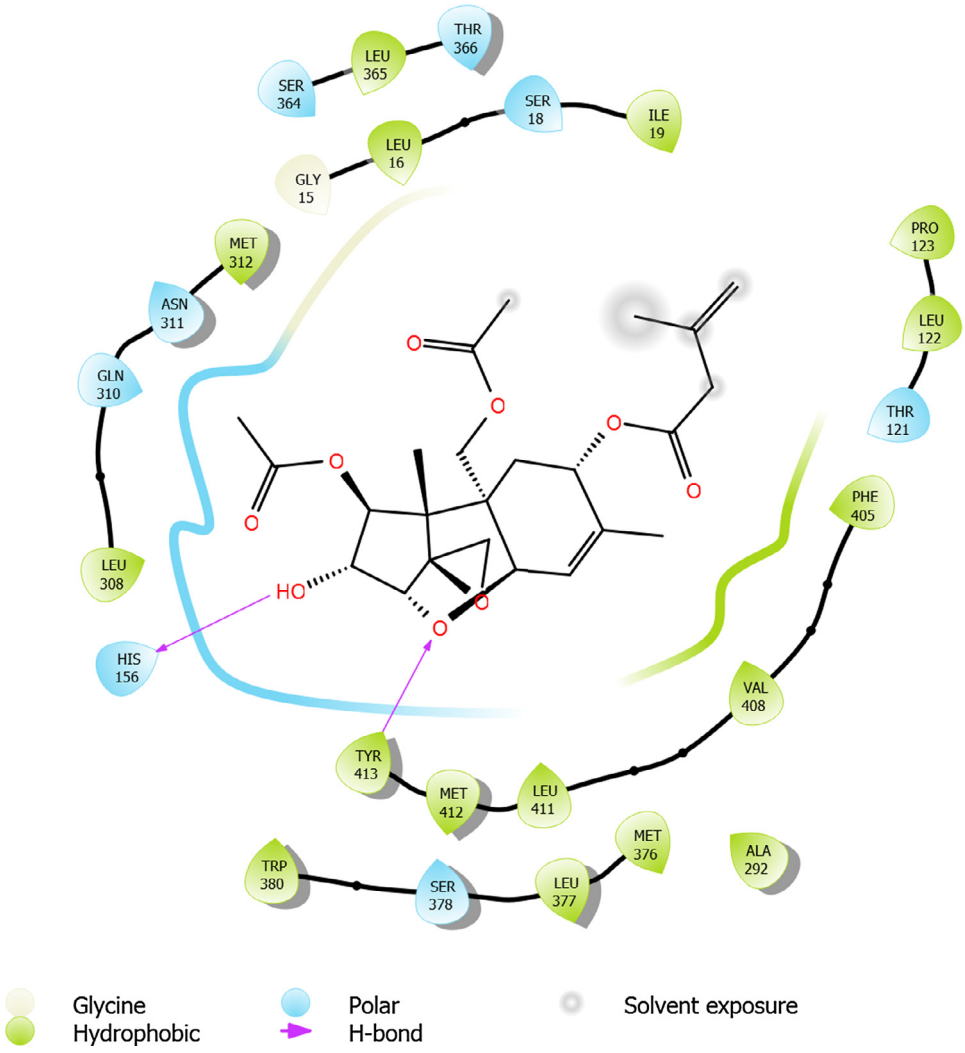

Fig. 12. Two dimensional ligand interaction diagram of the native ligand, ZBA with the target.

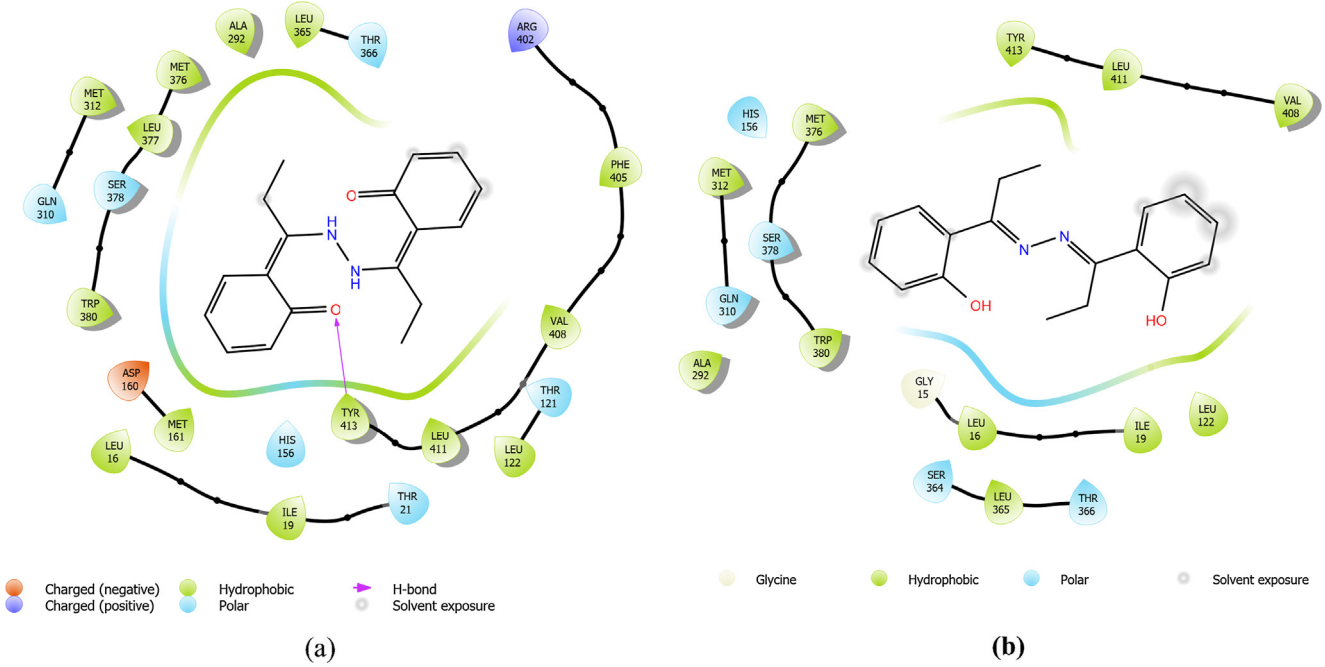

Fig. 13. Two dimensional ligand interaction diagram of (a) keto–amine and (b) phenol–imine forms with the target.

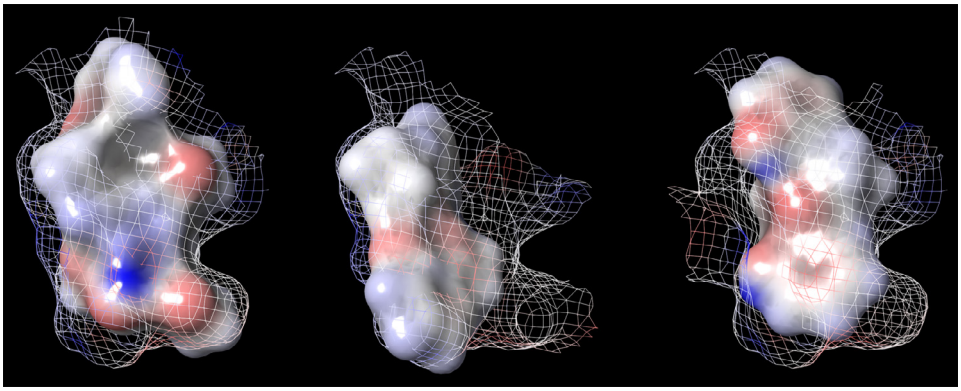

Fig. 14. Binding surface of the target together with ZBA (left), keto–amine (right) and phenol–imine (middle) forms.

rotates freely but upon binding, this rotation is relatively restricted which results in the loss of rotational entropy and this would correspond to a penalty in the estimated docking/MMGBSA energy.

4. Conclusions

In the present work, 2,2′(hydrazine-1,2-diylidenebis(propan-1-yl-1-ylidene))diphenol was synthesized and characterized by X-ray diffraction and IR, NMR spectroscopic methods. In experimental studies and in theoretical calculations, the phenol-imine structure was found to be more stable than the keto-amine structure. Promising *in vitro* antifungal activities were observed especially towards *A. solani*. Although theoretical calculations showed that the phenol-imine form was more stable, molecular docking calculations pointed out that the keto-amine form had critical binding interactions with the potential target. The loss of rotational entropy resulted from the restriction of free rotation of phenol group in phenol-imine form upon binding would correspond to a penalty in the estimated docking/MMGBSA energy. Both tautomeric forms were predicted to obey drug likeness properties. The results obtained here from both experimental and computational methods might serve as a potential lead in the development and optimization of novel anti-fungal agents.

Acknowledgement

This study was supported financially by the Research Centre of Ahi Evran University (**PYO-MUH.4001.15.004**). In addition, the numerical calculations reported in this paper were partially performed at TUBITAK ULAKBIM, High Performance and Grid Computing Center (TRUBA resources).

References

[1] T. Karakurt, A. Cukurovali, N.T. Subasi, I. Kani, J. Mol. Struct. 1125 (2016) 433.
[2] V. Macho, M. Králik, J. Hudec, J. Cingelova, J. Mol. Catal. A: Chem. 209 (2004) 69.
[3] S. Issaadi, T. Douadi, A. Zouaoui, S. Chafaa, M. Khan, G. Bouet, Corros. Sci. 53 (2011) 1484.
[4] K.H. Reddy, P.S. Reddy, P.R. Babu, Transition Met. Chem. 25 (2000) 505.
[5] D. Hadjipavlou-Litina, A. Geronikaki, Arzneimittelforschung 46 (1996) 805.
[6] B.S. Holla, K. Malini, B.S. Rao, B. Sarojini, N.S. Kumari, Eur. J. Med. Chem. 38 (2003) 313.
[7] A. Jarahpour, M. Motamedifar, K. Pakshir, N. Hadi, M. Zarei, Molecules 10 (2004) 815.
[8] G. Rauhut, S. Puyear, K. Wolinski, P. Pulay, J. Phys. Chem. 100 (1996) 6310.
[9] P. Hohenberg, W. Kohn, Phys. Rev. B 136 (1964) B864.
[10] W. Kohn, L.J. Sham, Phys. Rev. 140 (1965) 1133.
[11] R.A. Gaussian09, Inc., Wallingford CT, 2009.
[12] R. Dennington, T. Keith, J. Millam, Semichem Inc., Shawnee Mission, KS, 2009.
[13] S. Baroni, A. dal Corso, S. de Gironcoli, P. Giannozzi, C. Cavazzoni, et al., Available from: <http://www.democritos.it/>.
[14] A. Bruker, APEX2, V2008. 6, SADABS V2008/1, SAINT V7. 60A, SHELXTL V6. 14. Bruker AXS Inc., Madison, Wisconsin, USA, 2008.
[15] G.M. Sheldrick, Acta Crystallogr. Sect. A 70 (2014) C1437.
[16] G.M. Sheldrick, Acta Crystallogr. Sect. C: Struct. Chem. 71 (2015) 3.
[17] O.V. Dolomanov, L.J. Bourhis, R.J. Gildea, J.A.K. Howard, H. Puschmann, J. Appl. Crystallogr. 42 (2009) 339.
[18] C.F. Macrae, I.J. Bruno, J.A. Chisholm, P.R. Edgington, P. McCabe, E. Pidcock, L. Rodriguez-Monge, R. Taylor, J.v. Streek, P.A. Wood, J. Appl. Crystallogr. 41 (2008) 466.
[19] A.D. Becke, J. Chem. Phys. 98 (7) (1993) 5648.
[20] C. Lee, W. Yang, R.G. Parr, Phys. Rev. B 37 (1998) 785.
[21] M. Jamróz, J.C. Dobrowolski, J. Mol. Struct. 565 (2001) 475.
[22] J.P. Perdew, A. Zunger, Phys. Rev. B 23 (1981) 5048.
[23] Schrödinger Release 2017-1, LLC, New York, NY, 2017.
[24] Schrödinger Release 2017-1: QikProp, Schrödinger, LLC, New York, NY, 2017.
[25] M.O. Nwosu, J.I. Okafor, Mycoses 38 (1995) 191.
[26] A. Onaran, M. Yılar, J. FoodAgri. Environ. 10 (2012) 287.
[27] D. Pandey, N. Tripathi, R. Tripathi, S. Dixit, Zeitschrift für Pflanzenkrankheiten und Pflanzenschutz/J. Plant Dis. Protect. (1982) 344.
[28] S. Chantrapromma, P. Jansrisewangwong, H.-K. Fun, Acta Crystallogr. Sect. E: Struct. Rep. Online 66 (2010) o2994.
[29] H.-K. Fun, P. Jansrisewangwong, C. Karalai, S. Chantrapromma, Acta Crystallogr. Sect. E: Struct. Rep. Online 67 (2011) o3424.
[30] I. Alkorta, R.M. Claramunt, J. Elguero, M.B. Ferraro, J.C. Facelli, P.F. Provasi, et al., J. Mol. Struct. 1075 (2014) 551.
[31] J.P. Merrick, D. Moran, L. Radom, J. Phys. Chem. A 111 (2007) 11683.
[32] H.A. Dabbagh, A. Teimouri, A.N. Chermahini, M. Shahraki, Spectrochim. Acta Part A Mol. Biomol. Spectrosc. 69 (2008) 449.
[33] Ç. Yüksektepe, N. Çalişkan, I. Yilmaz, A. Çukurovali, J. Chem. Crystallogr. 40 (2010) 1049.
[34] H. Tanak, J. Phys. Chem. A 115 (2011) 13865.
[35] Ö. Tamer, D. Avcı, Y. Atalay, Spectrochim. Acta Part A Mol. Biomol. Spectrosc. 117 (2014) 78.
[36] R. Bayrak, H.T. Akçay, M. Pişkin, M. Durmuş, İ. Değirmencioğlu, Dyes Pigm. 95 (2012) 330.
[37] G. Varsányi, Assignments for Vibrational Spectra of Seven Hundred Benzene Derivatives, Halsted Press, 1974.
[38] K. Furić, V. Mohaček, M. Bonifačić, I. Štefanić, J. Mol. Struct. 267 (1992) 39.
[39] D. Avcı, Y. Atalay, M. Şekerci, M. Dinçer, Spectrochim. Acta Part A Mol. Biomol. Spectrosc. 73 (2009) 212.
[40] J. Mohan, Organic Spectroscopy: Principles and Applications, Crc Press, 2004.
[41] R. Ditchfield, J. Chem. Phys. 56 (1972) 5688.
[42] P. Pulay, K. Wolinski, J. Hinton, J. Am. Chem. Soc. 112 (1990) 8251.
[43] P. Atkins, Paula J. Atkins', Physical Chemistry, WH Freeman and Company, New York, 2006.
[44] C. Selvaraj, S.K. Singh, J. Biomol. Struct. Dyn. 32 (2014) 1333.
[45] R.F. Bader, Chem.-A Eur. J. 12 (2006) 2896.
[46] I. Rozas, I. Alkorta, J. Elguero, J. Am. Chem. Soc. 122 (2000) 11154.
[47] T.A. Keith, AIMAll (Version 15.09.27), T.K. Gristmill Software, Overland Park K. S., USA, 2016.
[48] E. Espinosa, E. Molins, C. Lecomte, Chem. Phys. Lett. 285 (1998) 170.
[49] Schrödinger Release 2017-1: Maestro, Schrödinger, LLC, New York, NY, 2017.
[50] E. Harder, W. Damm, J. Maple, C. Wu, M. Reboul, J.Y. Xiang, L. Wang, D. Lupyan, M.K. Dahlgren, J.L. Knight, J. Chem. Theory Comput. 12 (2015) 281.
[51] T.A. Halgren, R.B. Murphy, R.A. Friesner, H.S. Beard, L.L. Frye, W.T. Pollard, J.L. Banks, J. Med. Chem. 47 (2004) 1750.
[52] R.A. Friesner, J.L. Banks, R.B. Murphy, T.A. Halgren, J.J. Klicic, D.T. Mainz, M.P. Repasky, E.H. Knoll, M. Shelley, J.K. Perry, J. Med. Chem. 47 (2004) 1739.
[53] Prime, Version 3.0, Schrödinger, LLC, New York, NY, 2011
[54] D. Bashford, D.A. Case, Annu. Rev. Phys. Chem. 51 (1) (2000) 129.
[55] V. Tsui, D.A. Case, Biopolymers 56 (4) (2000) 275.
[56] J. Li, R. Abel, K. Zhu, Y. Cao, S. Zhao, R.A. Friesner, Proteins 79 (2011) 2794.

[57] C.A. Lipinski, F. Lombardo, B.W. Dominy, P.J. Feeney, Adv. Drug Deliv. Rev. 23 (1997) 3.
[58] D.F. Veber, S.R. Johnson, H.Y. Cheng, B.R. Smith, K.W. Ward, K.D. Kopple, J. Med. Chem. 45 (2002) 2615.
[59] A. Ece, F. Sevin, Lett. Drug Des. Discovery 7 (9) (2010) 625.
[60] A. Ece, F. Sevin, Med. Chem. Res. 22 (2013) 5832.
[61] A. Ece, Turkish J. Pharm. Sci. 13 (2) (2016) 241, https://doi.org/10.4274/tjps.28290.
[62] H. Tahtaci, H. Karacık, A. Ece, M. Er, M.G. Şeker, Mol. Inf. (2017), https://doi.org/10.1002/minf.201700083.
[63] C. Yamali, H.I. Gul, A. Ece, P. Taslimi, I. Gulcin, Chem. Biol. Drug Des. (2017), https://doi.org/10.1111/cbdd.13149.